Three-Dimensional Inviscid Flow in Mixers, Part II: Analysis of Turbofan Forced Mixers

T. J. Barber*
United Technologies Research Center, East Hartford, Connecticut
G. L. Muller† and S. M. Ramsay‡
Pratt & Whitney Aircraft Group, East Hartford, Connecticut
and
E. M. Murman§
Massachusetts Institute of Technology, Cambridge, Massachusetts

A three-dimensional potential analysis has been formulated and applied to the inviscid flow over a turbofan forced mixer. In Part I, a unique small-disturbance formulation for the analysis of the inviscid flow in forced mixer configurations was presented. The method reduced the governing equations by using a flux volume formulation along a Cartesian grid. In Part II, the method is extended to include the effects of power addition within the potential formulation. Calculations are presented for practical turbofan mixer configurations. Comparison calculations are also presented with measured surface pressure distributions and measured axial velocity profiles.

Nomenclature

A = area of elemental face
C_p = pressure coefficient
g_k = kth component of axisymmetric perturbation potential
h_k = kth component of angular portion of perturbation potential
L = axial length of mixer lobe
M = Mach number
n = normal component
NH = number of flux equations solved
NF = number of Fourier terms in geometry
p = static pressure
R_m = mean radius
x,r,θ = cylindrical coordinates
u,v,w = velocity components
γ = specific heat ratio
Γ = circulation at lobe trailing edge
λ_k = kth Fourier component of lobe surface
ν = compound flow indicator
ψ = perturbation velocity potential

Subscripts and Superscripts

i,j = (x,r) difference indices
k = Fourier harmonic component
U,L = upper and lower components, respectively, of flux element
x,r,θ = partial derivatives in (x,r,θ) coordinates
0 = stagnation property
∞ = inlet property

Received Aug. 5, 1985; revision received Jan. 22, 1986.

*Senior Research Engineer. Member AIAA.
†Senior Research Analyst. Member AIAA.
‡Analyst.
§Professor, Aeronautics & Astronautics. Member AIAA.

Introduction

A FORCED mixer is a device used in gas turbine engines to internally mix the hot core or primary gas stream with the cold fan bypass or secondary stream. In commercial applications this mixing process can produce a thrust increment; however, this benefit can frequently be negated by the added weight of the increased cowl length and added pressure losses. Conventional installations have usually avoided this tradeoff and resorted to separate flow nacelles. In such applications, any energy recovery is lost to the ambient flow. When engine cycles are appropriately optimized the energy recovery potential is extremely small, but when growth or derivative engine configurations are considered, the tradeoff between increased mixing efficiency and loss penalties is improved through the use of forced mixers. Conventional or commercial forced mixer configurations consist of a periodic lobe structure. In general, the lobe trailing edge may be scarfed or scalloped to enhance its performance. The scarf or lobe cutback angle is used to reduce lobe length with increasing penetration into the core. Scalloping is a cutout of the lobe lateral surface used to minimize lobe wall structural problems while promoting tangential mixing.

Recently, "benchmark" experiments[1,2] have utilized high response and laser Doppler velocimeter (LDV) instrumentation to probe the mixing chamber in an attempt to explain the driving mechanisms of the mixing process. These experiments have confirmed that the mixing process is an inviscid-dominated process, and that the primary driving mechanism is the secondary flow generated in the lobed region of the flow. Several researchers have proposed a variety of inviscid and viscid processes for producing the secondary flow, but, as yet, no attempt has been made to model them analytically. Anderson et al.[3] and Anderson and Povinelli[4] have lumped these terms together under a "generic" vorticity label, analytically simulating its effect in terms of a vortex sheet distributed along the lobe exit surface. Such an approach has been used to generate inlet conditions for a viscous marching analysis in the mixing duct. The results of these calculations have been shown to realistically simulate observed flow mixing patterns. The purpose of this paper is to develop an inviscid analysis which, in

conjunction with a lobe boundary-layer analysis, can predict the flow over the mixer lobes, thereby obtaining the conditions needed to initiate a marching viscous calculation in the downstream duct.

One particular inviscid secondary vorticity generator is called the "flap" vorticity scheme. In this model, the vorticity is associated with the periodic lift distribution (Fig. 1) produced by the periodic lobe trailing edge, which resembles a series of flaps about a mean surface. The feasibility of an inviscid method predicting an observed level of flow penetration is dependent on the axial-flow component remaining attached at the surface. Surface pressure distributions and shed vorticity strength therefore represent parameters for calibrating the analysis presented in Part I.

Analysis Overview

An inviscid small-disturbance potential-flow analysis was formulated in Part I of this paper.[5] The method is applicable to axially slender lobe geometries having local flow Mach numbers low enough so that a perturbation or small-disturbance approach can be utilized. The nondimensionalized mass flux vector in the conservation laws is then given by

$$\rho\vec{v}=(1+\beta^2\varphi_x)\vec{i}_x+\varphi_r\vec{i}_r+\frac{1}{r}\varphi_\theta\vec{i}_\theta \tag{1}$$

where $\beta^2=1-M_\infty^2$ and φ is the perturbation potential. With these restrictions and careful treatment of the conservation laws and boundary conditions, one can uncouple the θ dependence in the problem from the axial dependence by expressing the perturbation potential as

$$\varphi(x,r,\theta)=\sum_{k=1}^{N} g_k(x,r)h_k(\theta) \tag{2}$$

where the subscript k refers to the separated or Fourier modes of the solution. The axisymmetric governing equations are then discretized using a finite-volume algorithm on a Cartesian grid and reduced to a linear system of equations for g_k. The forcing terms for the boundary effect are the slopes of the corresponding Fourier modes λ_k of the lobe surface.

The analysis, as formulated in Part I, defines a unique set of inflow conditions for an idealized mixer-type geometry by using an appropriately formulated Kutta condition. In more realistic turbofan installations these conditions must be modified to reflect the effects of power addition and possible fan nozzle flow choking.

Inlet Flow Boundary Conditions

Flow requirements for cruise engine operating conditions are typically determined by engine power settings as well as by inlet and nozzle exit areas. Analysis of the localized mixer/nozzle problem requires a completely specified set of boundary conditions, however, precautions must be taken to avoid specifying inconsistent fan and engine core flow conditions such that the Kutta condition at the lobe trailing edge cannot be satisfied. The problem is further complicated when one wishes to generalize the analysis so that it is capable of addressing either choked or unchoked conditions at the nozzle exit plane. In effect, the nozzle exit plane sets the net flow rate while the Kutta condition defines the flow split between the fan and engine streams. For example, if the onset flows were specified in terms of p_0, T_0, and M_∞, as shown schematically in Fig. 2, the problem could be overdefined. A uniquely defined system can be constructed using the nozzle exit flow conditions in conjunction with the wake contact surface matching conditions to determine the fan and core flow requirements.

The analysis developed in the following section is based on a compound nozzle model, wherein the curvature-induced transverse pressure gradients are neglected and the static pressure is assumed to be only a function of axial position. Approximating the nozzle exit flow by a quasi-one-dimensional flow, the continuity equation and the isentropic forms of the energy equation for a single flow can be combined to give

$$\frac{dA}{dx}=\frac{A}{\gamma}\left(\frac{1}{M^2}-1\right)\frac{d}{dx}(\ell n p) \tag{3}$$

This equation has been generalized[6] for multistream flows, where quasi-one-dimensional matching conditions across each dividing streamline prevent mixing but do ensure pressure continuity across the flow. Bernstein et al.[6] also demonstrated that the nozzle flow exit state corresponds to the sign of ν, the compound flow indicator, i.e.,

$$\nu=\sum_i \frac{A_i}{\gamma}\frac{1}{M_i^2}-1 \tag{4}$$

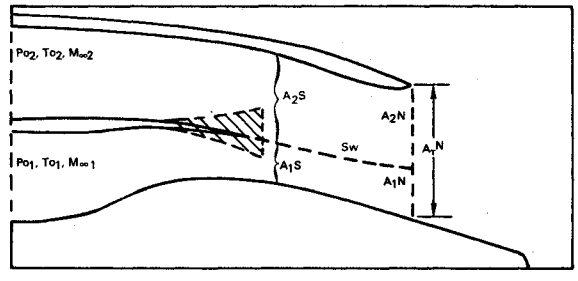

Fig. 2 Dual stream choked flow domain.

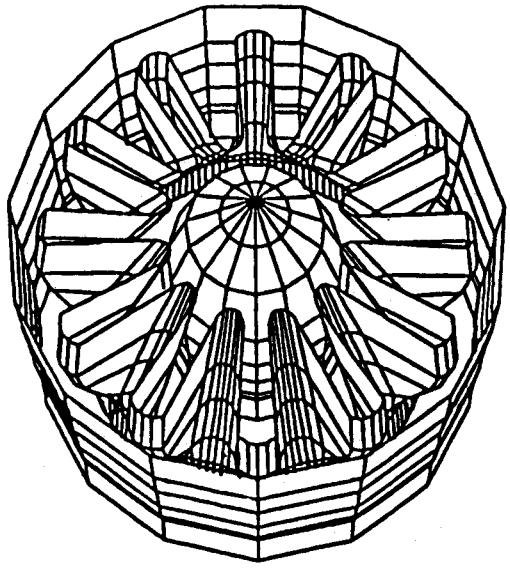

Fig. 3 Three-dimensional display of JT8D-209 mixer geometry.

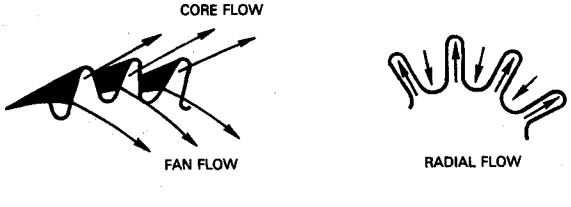

Fig. 1 Secondary flow generation turning or flap vorticity model.

where

$\nu > 0$ compound subsonic

$\nu = 0$ compound sonic

$\nu < 0$ compound supersonic

Equation (4), in conjunction with the definition of the local mass flows, in terms of their stagnation properties, is sufficient to provide closure of the problem. The analysis is applied at the nozzle exit plane and subsequently at the inlet plane. An iteration is necessary to determine the individual flows. This directly determines g_x, the "velocity" for each stream at the downstream plane of the computational domain. In the present analysis it is assumed that $g_x = g_{x_0}$, while all higher modal derivatives at the inlet plane are identically zero.

Kutta Condition—Powered Wake Analysis

Treatment of the flow downstream of the mixer lobe must allow for the interaction of the core and fan flows. Even in nonpowered situations, an induced or secondary flowfield is generated and convected from the lobe trailing edge as a jump in potential. This jump will remain constant and convect along the trailing-edge streamline. In the situation of power addition, both streams are assumed locally irrotational with different energy levels. They inviscidly interact through the potential jump that is locally determined from the basic consistency conditions across a contact discontinuity, i.e., static pressure match on the wake or vortex sheet S_w and streamline slope continuity

$$\vec{v} \cdot \vec{n} = 0 \text{ on } S_W^+, S_W^-$$

Classical linear theory assumes that the wake lies along a constant radius surface (R_m) from the trailing edge. In the current model, the streamline slope condition is relaxed by assuming, consistent with the surface boundary condition formulation, that the wake can be modeled as an axisymmetric surface that is either a constant radius surface or varies with axial position. In the analysis previously derived in Part I, it was suggested that the actual wake streamline path could be determined iteratively. In the present constant radius model, the flow is permitted to cross through the wake to satisfy the consistency conditions. The flux balance for the wake is expressed in terms of a mean potential $\bar{g}_k$ and a locally varying potential jump $[g]_k$, i.e.,

$$\bar{g}_{i,j,k} = \tfrac{1}{2}(g^U_{i,j,k} + g^L_{i,j,k}) \tag{5a}$$

$$[g_k]_{ij} = (g^U_{i,j,k} - g^L_{i,j,k}) \tag{5b}$$

The potential jump is obtained by applying the constraints of static pressure and streamline slope continuity. Generalization of this analysis for powered flows is possible by expressing the pressure match identity in terms of the local pressure coefficients referenced to the same freestream static pressure. Therefore, the pressure coefficient C_p match becomes

$$C_p^U = \frac{\gamma_L M^2_{\infty L}}{\gamma_U M^2_{\infty U}} C_p^L + \frac{2\Delta p_\infty}{\gamma_U M^2_{\infty U}} \tag{6}$$

A linearized C_p model then can be used to separate out the axisymmetric component of each model ($\bar{C}_{p_k}$).

$$\bar{C}_{p_k}(r,x) = -2g_{x_k}(r,x) \tag{7}$$

At the lobe trailing edge, Eqs. (6) and (7) are equivalent to separate Kutta conditions for each mode. The streamline slope matching conditions along the general wake contour can also be simplified by assuming that the axial velocity perturbation is small relative to the freestream velocity and that the wake follows the constant radius approximation.

Equations (5-7) are then combined to determine the potential jump

$$[g_k]_x = E_1 \delta_{0k} + E_2 \bar{g}_{x_k} \tag{8}$$

where δ_{0k} is the Kronecker delta function. Ideally, the jump in potential along the wake is obtained by integrating out axially from the trailing edge along the mean radius as follows:

$$[g_k]_{ij} = E_1 \delta_{0k}(x - x_{\text{TE}}) + E_2 g_{k_i} + \{[g_k] - E_2 \bar{g}_k\}_{\text{TE}} \tag{9}$$

In the entire preceding discussion, the wake slope was assumed given. In principle, the path should be evolved iteratively. A simple streamline tracing procedure could be used to update the wake path periodically.

The power effect on the downstream flow can be described in terms of a simple integral parameter, the circulation Γ of the induced secondary flow. By an appropriate choice of integration domain

$$\Gamma = [\varphi]_{\theta=0} - [\varphi]_{\theta=\theta_0} \tag{10}$$

Eq. (10) can be re-expressed in terms of the separated variables as follows:

$$\Gamma = 4 \sum_{k=1}^{NH/2} (\bar{g}_{2k} \Delta U_\infty - [g_{2k}] \bar{U}_\infty)_{\text{TE}} \tag{11}$$

where only the odd modes contribute to the net induced circulation field.

Geometry Definition

General lobe contour definition can be a complex problem even if scalloping and scarf angle cutouts are not included. Current commercial designs fall within three general categories: radial, parallel, or circular-arc sidewalls, with the remaining segments of the lobe defined in terms of tangentially intersecting circular-arc segments. Considering the periodic nature of the analysis formulated in Part I, one

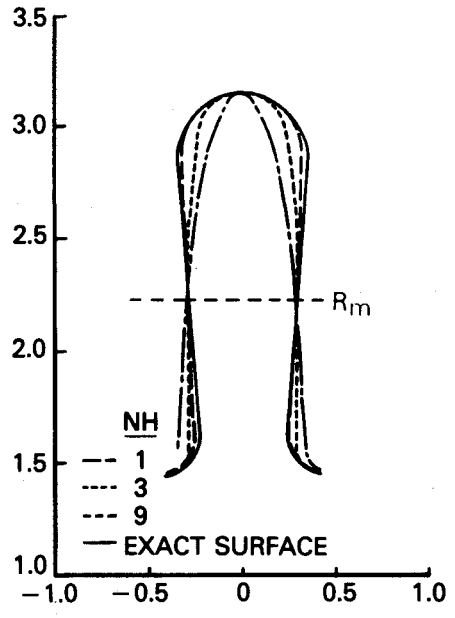

Fig. 4 Comparison of Fourier modal reconstruction of JT8D lobe near trailing-edge plane.

must limit the geometry capability to axisymmetric duct wall configurations while the lobe cross section must avoid sidewall geometries which are multivalued in the radial coordinate. Using this approach, a mixer centerbody and fan cowl can be defined and replicated using the Brigham Young University Movie Three-Dimensional Hidden Line Graphics Program to produce Fig. 3.

A measure of the feasibility of the Fourier decomposition method can be demonstrated by considering a finite number of harmonics and comparing the reconstructed lobe to the given lobe definition. An equal angle series construction permits use of a fast Fourier transform (FFT) scheme to evaluate the Fourier coefficients. The reconstructed lobes are shown in Fig. 4 for three levels of approximation ($NH=1$, 3, and 9). The base contour was generated analytically using 50 points. The modal analyses demonstrate varying degrees of agreement, with the largest excursions in all approximations occurring at points where the curvature changes instantaneously. Whereas this aspect is commonly found in square wave reconstructions, where a *large* number of modes must be used to obtain an accurate wave representation, the slight lobe contour mismatch should not be significant in establishing the magnitude of the "flap" vorticity field. The sensitivity of the analysis to the number of modes, however, will subsequently be shown to be a critical factor in determining the mean radius—the leading term obtained from the FFT analysis.

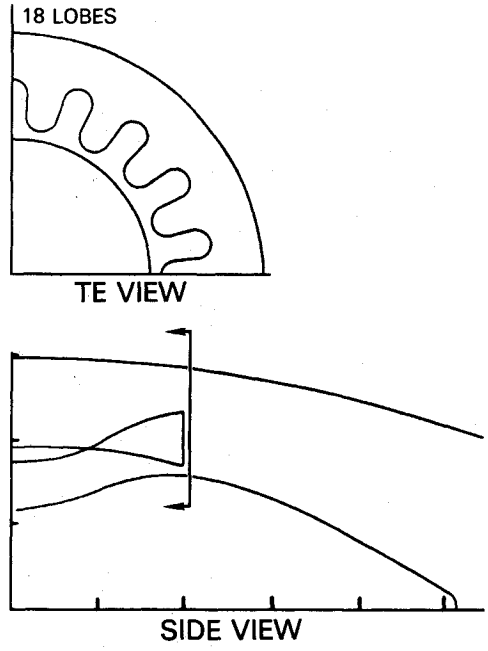

Fig. 5 E^3 configuration 29-lobe mixer.

Results and Discussion

The mixer analysis (FLOMIX) was described in detail and calibrated for a model problem in Part I of this paper. More realistic applications of the method can be studied by considering flight-type configurations. In particular, two specific powered applications are presented because both have "benchmark" experimental data available for comparison: 1) 18-lobe Energy Efficient Engine (E^3) configuration 29 forced mixer,[7,8] and 2) 12-lobe JT8D-209 forced mixer.[2] The E^3 configuration (Fig. 5) is well suited for an analytical comparison although it was designed for a modern high-bypass engine; the lobes were built specifically for code verification, i.e., the lobes were not scalloped or scarfed and extensive surface static pressure surveys were made in the lobe region of the mixer. In contrast, the JT8D-209 forced mixer design, typical of first-generation low-bypass applications, has higher penetration lobes with a 12-deg scarf angle. While this geometry is not strictly suitable for code comparison, the experimental data included three-component LDV velocity profile measurements at the lobe trailing edge. Satisfactory modeling of these lobe cross sections, even for the JT8D-209 high-penetration lobe (Fig. 4), is possible with only ten or more Fourier terms; however, a more complete discussion relating to the specific value for NH is given below.

Postprocessing of the potential solution produces a complete definition of the surface Mach number and quantifies the level of "flap" vorticity or circulation through the potential jump at the lobe trailing edge. The surface solutions, although strictly determined along the approximate mean surfaces, can be interpreted, to first order, as solutions on the actual surfaces. By examining the potential jump variable, an effort will be made to quantify separately the contributive effects of mean flow turning, power addition, and lobe aspect ratio (penetration angle) on the overall mixing process.

Numerical solutions initially are made for the E^3 configuration 29-lobe mixer and compared to test data measured on a full-scale model at FluiDyne Engineering Corp. The experimental cruise flow conditions were characterized by power settings of $\Delta p_0/p_{0s}=0.094$ and $\Delta T_0/T_{0s}=1.50$, where s refers to reference conditions in the secondary or fan stream, and Δ refers to the difference in state between the fan and engine streams. Numerical simulation of the measured flow conditions is obtained by setting the upstream total conditions in each stream while also specifying the nozzle exit plane static pressure. The quasi-one-dimensional choked flow analysis correctly sets up a choked flow at the nozzle exit plane and establishes inlet mass flows and flow Mach numbers to within 10% of those measured by the facility flowmeters.

The dependence of the solution on the level of modal approximation still needs to be answered. Table 1 summarizes the individual modal potential jumps $[g_k]$ obtained from a series of calculations in which different levels of modal approximation ($NH=0,1,2,3,...$) were used to simulate the E^3 mixer. The calculations were initially made for an axisymmetric mode only so that the effect of flow turning of the

Table 1 Potential jump comparisons $[g_k]$

				$k=$					
NH	NF	Power addition	Total jump	0	1	2	3	4	5
0	axi (18)	No	−0.093	−0.093					
0	axi (18)	Yes	−0.012	−0.118	−0.093				
1	1	Yes	−0.396	−1.328	−0.068				
3	3	Yes	−0.527	−0.467	−0.084	0.018	0.006		
5	5	Yes	−0.353	−0.292	−0.087	0.013	0.007	0.006	
3	5	Yes	−0.367	−0.293	−0.087	0.013			
5	9	Yes	−0.263	−0.187	−0.088	0.008	0.009	−0.004	−0.003
Asymptotic value ($NH=5$, $NF=18$)			−0.191	−0.118	−0.089	0.008	0.010	−0.002	−0.003

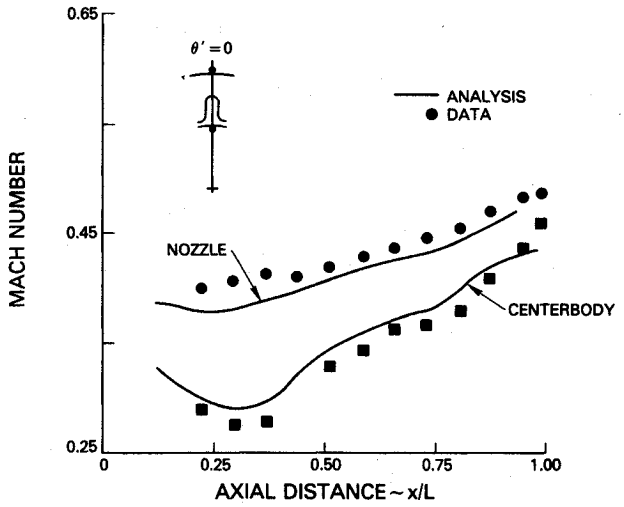

Fig. 6 Surface Mach number comparisons for E^3 duct walls at lobe crest orientation.

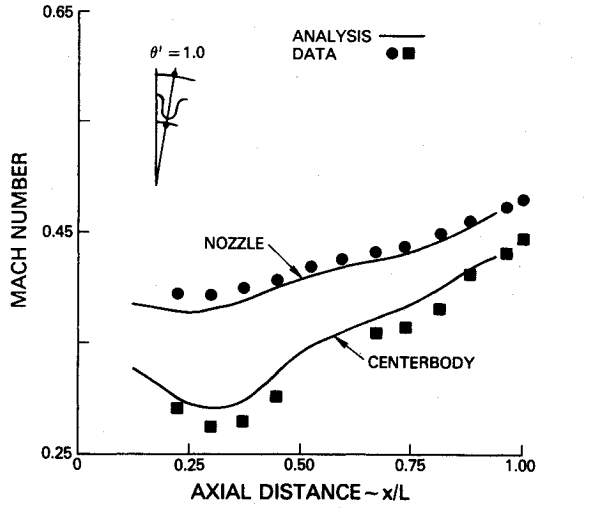

Fig. 8 Surface Mach number comparisons for E^3 duct walls at lobe trough orientation.

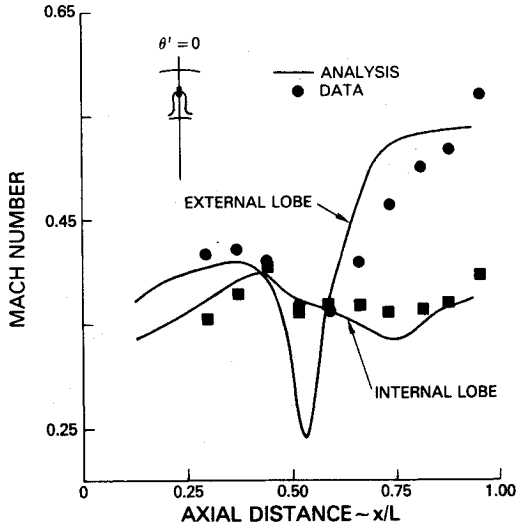

Fig. 7 Surface Mach number comparisons for E^3 mixer lobe at lobe crest orientation.

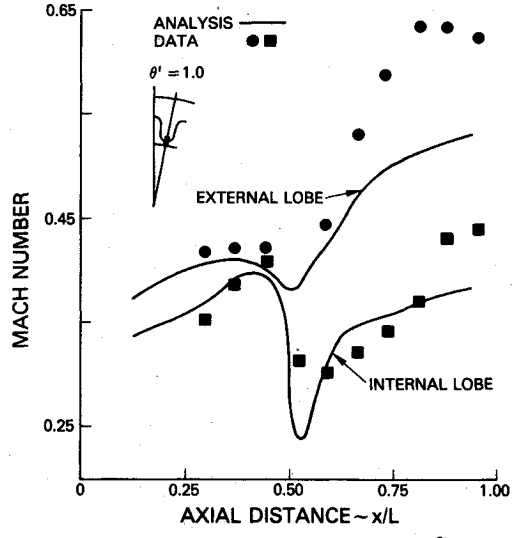

Fig. 9 Surface Mach number comparisons for E^3 mixer lobe at lobe trough orientation.

onset axial flow by the axisymmetric component (-0.093) and power addition (-0.012) could be identified. With the mean radius having a positive trailing-edge angle, these results demonstrate that a positive circulation corresponds to a clockwise rotation. The tabulated calculations varied both the number of harmonic terms (NH) used to represent the θ dependence of the velocity potential and the number of Fourier terms (NF) used to represent the θ dependence of the lobe surface. The tabulated results indicate that, while each approximation produces different total and modal potential jumps, the individual modes approach fixed values as more terms are included. Although the higher modal solutions converge much more rapidly than the leading terms, the additional storage required for these higher-order terms is impractical. A study of the governing differential equations indicates that the modal coupling is extremely weak for the axisymmetric mode and that its primary driving term is the mean radius, determined from the Fourier analysis. Since higher-order solutions (NH large) contribute little to the total circulation field, one can neglect these equations while retaining the addition terms for an improved Fourier (NF) definition of the lobe and, more importantly, the mean radius. For example, calculations with $NH=3$ and $NF=5$ yield the same modal jumps as $NH=5$ and $NF=5$. In the comparisons described below the solution parameters $NH=5$ and $NF=18$ were used as representative of an "asymptotic" solution.

Surface Mach number calculations, compared to measured data within the lobe region, are shown in Figs. 6-9. Figures 6 and 7 present comparisons made for an azimuthal cut aligned with the lobe crest, whereas Figs. 8 and 9 show comparisons for the lobe trough orientation. Initial calculations indicated that the quasi-one-dimensional boundary condition set the flow and inlet conditions approximately 10% too high, therefore, a nozzle flow coefficient ($C_V=0.94$) was introduced to adjust the inlet flow conditions. With this modification good agreement between the present theory and data was obtained, as shown in Figs. 8 and 9. The axisymmetric fan nozzle and centerbody comparisons in Figs. 6 and 8 show little angular variation and are largely one-dimensional in behavior. The lobe surface solutions however have substantial θ dependence, as shown in Figs. 7 and 9. A major discrepancy in both of these figures is noted near $x/L=0.50$, the crossover point for the fan and core flows. The Mach number discrepancy at this point is produced primarily by the first modal solution in a manner similar to that predicted for the planar mixer case presented in Part I. Viscous interaction effects, however, should decrease analytically predicted gradients and reduce this mismatch.

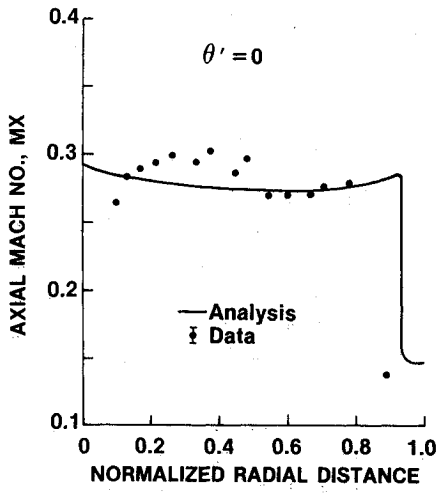

Fig. 10 Comparison of axial Mach number at lobe trailing-edge plane for JT8D-209 mixer, crest orientation.

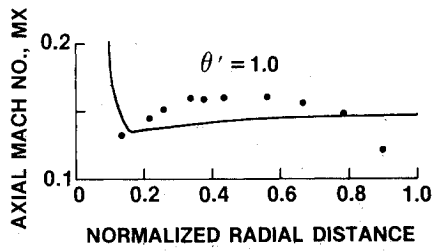

Fig. 11 Comparison of axial Mach number at lobe trailing-edge plane for JT8D-209 mixer, trough orientation.

The FLOMIX analysis has also been applied to the JT8D-209 lobe mixer configuration. This configuration was previously studied at United Technologies Research Center[2] in a scaled model test simulating the hot-flow ($\Delta p_0/p_{0s} = 0.044$, $\Delta T_0/T_{0s} = 1.617$) full-scale engine cruise conditions. Analysis of this configuration is complicated by the additional effect of a 12-deg scarf angle. While no surface or flowfield details were measured within the lobe region of the duct, LDV-measured velocity components were obtained just downstream of the lobe trailing edge and in the mixing duct. A comparison of results from the present theory with data, however, requires an interpretation of a small-disturbance solution off the mean radius. Examination of the Mach number profile at the lobe trailing edge indicates that the axial component is largely one-dimensional and has little variation with radius, within each stream. Shifting the surface flow solution to the physical lobe trailing edge results in comparisons for the radially measured axial component of Mach number, shown in Fig. 10 at the crest angular location and in Fig. 11 for the trough angular location. Both figures show good agreement between the FLOMIX analysis ($NH = 5$, $NF = 9$) and experiment.

A fuller interpretation of the flowfield at the lobe exit plane must be inferred from slender-body theory,[9,10] where the outer potential would be determined as a function of x from the solution of an axisymmetric problem and the inner potential would then be determined as a solution of the two-dimensional Laplace equation in the cross plane (r,θ). This philosophy will be used with the modal axisymmetric solutions to infer the cross-flow or inner solution.

Conclusions

A three-dimensional flow analysis for lobed forced mixers has been formulated. Although the analysis assumes that the flow processes are predominantly inviscid and can be applied only to slender mixer lobes ($\Delta R/L \ll 1$), the analysis is capable of recovering substantial features observed in an actual flowfield. In particular, calculations on flight-type mixers show good agreement between predicted and measured surface Mach number distributions. While these comparisons seem to indicate that viscous interaction effects would moderate predicted overspeed effects, they still confirm the basic inviscid nature of the lobe flow. Further comparisons of calculated and measured lobe exit profiles demonstrate that the FLOMIX analysis can be used effectively to generate realistic input profiles for a viscous marching calculation in the mixer duct.

Acknowledgments

The authors wish to thank the NASA Lewis Research Center for sponsoring this work. The program, Contract NAS3-23039, is under the direction of Mr. Allan Bishop. The authors also wish to thank Mr. D. Golden and Dr. W. C. Chin for their early contributions to the development of this analysis.

References

[1]Paterson, R. W. and Werle, M. J., "Turbofan Forced Mixer Flow Field," United Technologies Research Center, East Hartford, CT, UTRC R79-912924, 1979.

[2]Paterson, R. W., "Turbo Forced Mixer-Nozzle Internal Flow Field, I—A Benchmark Experimental Study," NASA CR 3492, 1982.

[3]Anderson, B. H., Povinelli, L. A., and Gerstenmaier, W. G., "Influence of Pressure Driven Secondary Flows of the Behavior of Turbofan Forced Mixers," AIAA Paper 80-1198, Jan. 1980.

[4]Anderson, B. H. and Povinelli, L. A., "Factors Which Influence the Behavior of Turbofan Forced Mixer Nozzles," AIAA Paper 81-0274, Jan. 1981.

[5]Barber, T. J., Muller, G. L., Ramsey, S. M., and Murman, E. M., "Three-Dimensional Inviscid Flow in Mixers—Part I: Mixer Analysis Using a Cartesian Grid," *Journal of Propulsion and Power*, Vol. 2, May-June 1986, pp. 275-281.

[6]Bernstein, A., Heiser, W., and Hevenor, C., "Compound Compressible Nozzle Flow," *Transactions of ASME, Journal of Applied Mechanics*, Ser. E, Vol. 3, pp. 549-554.

[7]Kozlowski, H. and Larkin, M., "Energy Efficient Engine Exhaust Mixer Model Technology Report," NASA CR-165459, 1981.

[8]Larkin, M. J. and Blatt, J. R., "Energy Efficient Engine Exhaust Mixer Model Technology Report Addendum—Phase III Test Report," NASA CR to be issued, 1984.

[9]Spreiter, J. R., "Aerodynamics of Wings and Bodies at Transonic Speeds," *Journal of the Aeronautical Sciences*, Vol. 26, No. 8, 1959, pp. 465-487.

[10]Malmuth, N. D., "An Asymptotic Theory of Wind Tunnel Wall Interference on Subsonic Slender Bodies," AIAA Paper 84-1625, 1984.